Facile Synthesis of Silver Nanoparticles Stabilized by Cationic Polynorbornenes and Their Catalytic Activity in 4-Nitrophenol Reduction

ARTICLE *in* LANGMUIR · MARCH 2013

Impact Factor: 4.46 · DOI: 10.1021/la305068p · Source: PubMed

4 AUTHORS, INCLUDING:

Bharat Baruah
Kennesaw State University
44 PUBLICATIONS **957** CITATIONS

SEE PROFILE

Gregory Gabriel
Oglethorpe University
16 PUBLICATIONS **832** CITATIONS

SEE PROFILE

Langmuir

Article

pubs.acs.org/Langmuir

Facile Synthesis of Silver Nanoparticles Stabilized by Cationic Polynorbornenes and Their Catalytic Activity in 4-Nitrophenol Reduction

Bharat Baruah,* Gregory J. Gabriel,* Michelle J. Akbashev, and Matthew E. Booher

Department of Chemistry and Biochemistry, Kennesaw State University, Kennesaw, Georgia 30144-5591, United States

Supporting Information

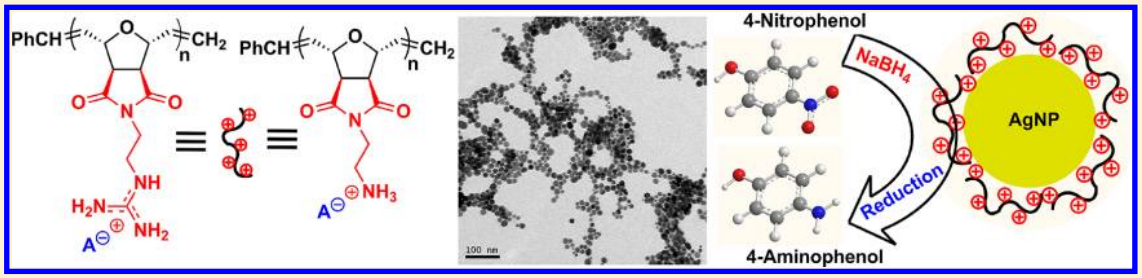

ABSTRACT: We report the facile one-pot single-phase syntheses of silver nanoparticles stabilized by norbornene type cationic polymers. Silver nanoparticles (AgNPs) stabilized by polyguanidino oxanorbornenes (PG) at 5 and 25 kDa and polyamino oxanorbornenes (PA) at 3 and 15 kDa have been synthesized by the reduction of silver ions with $NaBH_4$ in aqueous solutions at ambient temperature. The four different silver nanoparticles have been characterized by UV−vis spectroscopy, Fourier transform infrared spectroscopy (FTIR), dynamic light scattering (DLS), and transmission electron microscopy (TEM) for their particle size distributions. Interestingly, PG stabilizes the silver nanoparticles better than PA as evident from our spectroscopic data. Furthermore, the AgNP-PG-5K (5K = 5 kDa) was found to serve as an effective catalyst for the reduction of 4-nitrophenol to 4-aminophenol in the presence of $NaBH_4$. The reduction has a pseudo-first-order rate constant of 5.50×10^{-3} s^{-1} and an activity parameter of 1375 s^{-1} g^{-1}, which is significantly higher than other systems reported in the literature.

1. INTRODUCTION

In recent years, silver nanoparticles (AgNPs) have been gaining significant research interest due to their unique shape and size-dependent optical,[1] antimicrobial,[2] and catalytic properties.[3] Nanostructures of silver such as monodispersed nanoparticles,[4] nanoprisms,[5] nanocubes,[6] nanowires[7] and nanodisks[8] have potential applications in optics, catalysis, and SERS detection.[9]

The synthesis of silver nanoparticles involves three broadly defined routes. Silver nanoparticles can form in the presence of strong reducing agents, such as sodium borohydride,[10] hydrazine,[11] and tetrabutylammonium borohydride.[11] A second route can involve the UV irradiation,[12] γ-irradiation,[13] ultrasound irradiation,[14] or microwave[15] heating of silver ions in solution in the presence of capping agents. A third route involves prolonged heating of silver ions in solution in the presence of weak reducing agents, such as sodium citrate,[16] glucose,[17] dimethylformamide,[18] potassium bitartrate,[19] ascorbic acid,[20] and polyols.[21] A wide variety of capping agents have been used to control size, shape, stability, and solubility of silver nanostructures. Organic thiol compounds[22] are the most commonly used capping agents to stabilize colloidal silver. Long-chain amine,[23] aniline,[16] surfactant,[24] carboxylates,[4] and starch[25] have been also used to stabilize silver nanostructures. In addition, polymers such as poly(vinylpyrrolidone),[21] poly(amidoamine),[26] polyacrylate,[27] polyacrylonitrile,[28] and polyacrylamide[13] are also popular stabilizing agents. For example, Song et al.[29] used cationic polymer nanofibers to embed silver nanoparticles to reinforce the antimicrobial activity of the embedded silver nanoparticles. Tan and co-workers reported[12] the use of branched polyethylenimine (BPEI) and 4-(2-hydroxyethyl)-1-piperazineethanesulfonic acid (HEPES) together to reduce silver nitrate under UV irradiation for the synthesis of silver nanoparticles. The resultant silver nanoparticles are positively charged as the BPEI amino groups are protonated in the process.

In this report, the ability of two chemically different polynorbornenes to stabilize AgNPs was studied. The two cationic polymers, at two different molecular weights each, shown in Figure 1, were made from oxanorbornene monomers via ring-opening metathesis polymerization (ROMP) following reports by Tew and co-workers.[30,31] Polyguanidino oxanorbornene (PG) has been shown previously to have a remarkable combination of potent antimicrobial activity and low membrane-disruptive properties. Its amino counterpart, polyamino oxanorbornene (PA), interestingly does not possess these properties.[30] Additionally, the cell-permeating activities of

Received: December 20, 2012
Revised: February 27, 2013
Published: March 5, 2013

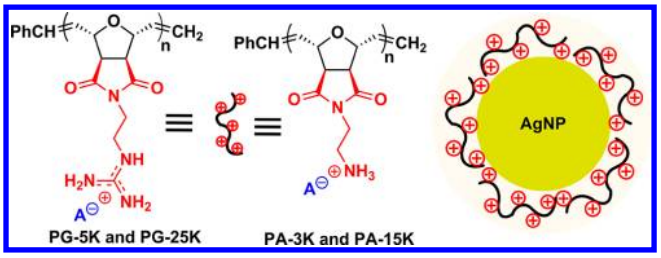

Figure 1. Structures of polyguanidino oxanorbornene (PG), polyamino oxanorbornene (PA), and a cartoon of the AgNP stabilized by PG or PA. Counteranion = trifluoroacetate. Two different molecular weights were targeted for each polymer, and the reported weights are of the Boc-protected polymers. For PG, made at 5 and 25 kDa, n = ∼10 and ∼54 and for PA, made at 3 and 15 kDa, n = ∼9 and ∼48.

polyarginines,[32,33] synthetic guanidinium-containing polymers,[34,35] and, in particular, the PG reported here[36] have recently led to the development of several other polynorbornene derivatives that efficiently act as protein transduction mimics.[37]

While several groups have fabricated and evaluated the antimicrobial properties of materials consisting of silver nanoparticles and cationic polymers such as polyvinylpyridines[38] and polyethylenimine,[39] there are no analogous studies in the literature using membrane-penetrating norbornene-type cationic polymers as stabilizing agents. Here we report the facile synthesis of silver nanoparticles stabilized by PA and PG as tracked with UV spectroscopy, IR spectroscopy, dynamic light scattering (DLS), and transmission electron microscopy (TEM). The size and the higher-order organization of the nanoparticles appear to be dependent on the type of cationic moiety present and the length of the polymer. Importantly, the silver nanoparticles synthesized in this report are also effective in catalyzing the reduction[40,41] of 4-nitrophenol to 4-aminophenol in the presence of excess $NaBH_4$ following pseudo-first-order kinetics. This reduction is unfeasible in the presence of the strong reducing agent, $NaBH_4$ without the nanoparticle catalyst. Since polyguanidino oxanorbornene (PG) is water-soluble and biocompatible,[30,37] PG-protected nanoparticles may be comfortably integrated into systems related to drug delivery, biomedical, pharmaceutical, and biosensor applications. Exploitation of such polymer-bound nanoparticles in the area of biomolecular and catalytic applications has tremendous potential in the development of nanotechnologies related to medicine.

2. EXPERIMENTAL SECTION

2.1. Materials. Solvents and chemicals for the monomer synthesis were purchased from Fisher Scientific. For the polymer synthesis the second-generation Grubbs catalyst, (tricyclohexylphosphine) (1,3-dimesitylimidazolidine-2-ylidine)benzylideneruthenium dichloride, was purchased from Aldrich and converted to a third-generation catalyst by reaction with 3-bromopyridine, from Aldrich, according to the literature. Polymerizations were performed in dry CH_2Cl_2 purchased sealed under nitrogen with molecular sieves from Acros. Silver nitrate, $AgNO_3$ (99%), was purchased from Fisher Scientific. $NaBH_4$ (98.5%) and 4-nitrophenol (98%) were purchased from Sigma-Aldrich.

2.2. Synthesis and Characterization of Polymers. The polyguanidino oxanorbornene samples at molecular weights of 5 and 25 kDa and the polyamino oxanorbornene samples at molecular weights of 3 and 15 kDa were synthesized according to the literature.[30,31] Gel permeation chromatography (GPC) was performed on the Boc-protected polymers with a Polymer Lab LC1120 pump equipped with a differential refractometer detector. The mobile phase used was THF with a flow rate of 1.0 mL/min at a temperature of 35 °C. Separations were performed with two Polymer Lab Resipore columns, and molecular weights were calibrated versus narrow molecular weight polystyrene standards. The reported weights of PG-5K, PG-25K, PA-3K, and PA-15K reflect the molecular weights of the Boc-protected polymers, and these polymers had an average degree of polymerization of 10, 54, 9, and 48, respectively. The GPC-derived PDI of the polymers as defined by M_w/M_n were all between 1.05 and 1.15, and proton NMR of the crude reaction mixtures indicated complete incorporation of the monomer into the polymer.

2.3. Synthesis of PG-5K Stabilized Silver Nanoparticles (AgNP-PG-5K). The PG-5K-stabilized AgNPs were synthesized as follows: 0.2 mL of $AgNO_3$ (100 mM) and 0.7 mL of PG-5K (2.5 mg/mL) solutions were thoroughly mixed in a 20 mL scintillation vial containing 8.95 mL of vigorously stirred water. 0.15 mL of fresh $NaBH_4$ solution in water (10 mM) was then slowly added into the mixed solution. The mixed solution immediately turned yellow upon the addition of $NaBH_4$, indicating the rapid formation of AgNP-PG-5K. The resulting AgNP-PG-5K solutions were left to stand overnight at room temperature to allow the residual $NaBH_4$ to decompose before any characterization took place. Polymer bound AgNPs were centrifuged in 1.5 mL Eppendorf tubes at 12 000 rpm for 20 min to remove unbound polymer and excess salts. After completion the supernatant was discarded, and the AgNP-PG-5K particles were redispersed in 1.0 mL of DI water.

2.4. Synthesis of PG-25K Stabilized Silver Nanoparticles (AgNP-PG-25K). The PG-25K-stabilized AgNPs were synthesized as follows: 0.2 mL of $AgNO_3$ (100 mM) and 0.4 mL of PG-25K (2.5 mg/mL) solutions were thoroughly mixed in a 20 mL scintillation vial containing 9.24 mL of vigorously stirred water. 0.16 mL of fresh $NaBH_4$ solution in water (10 mM) was then slowly added into the mixed solution. The mixed solution immediately turned yellow upon the addition of $NaBH_4$, indicating the rapid formation of AgNP-PG-25K. The resulting AgNP-PG-25K solutions were left to stand overnight at room temperature to allow the residual $NaBH_4$ to decompose before any characterization took place. Polymer bound AgNPs were centrifuged in 1.5 mL Eppendorf tubes at 12 000 rpm for 20 min to remove unbound polymer and excess salts. After completion the supernatant was discarded, and the AgNP-PG-25K particles were redispersed in 1.0 mL of DI water.

2.5. Synthesis of PA-3K and PA-15K Stabilized Silver Nanoparticles (AgNP-PA-3K and AgNP-PA-15K). The PA-3K- and PA-15K-stabilized AgNPs were synthesized following exactly the same procedures as described above for AgNP-PG-5K and AgNP-PG-25K, respectively. 0.7 mL of PA-3K (2.5 mg/mL) and 0.4 mL of PA-15K (2.5 mg/mL) were used instead of 0.7 mL of PG-5K (2.5 mg/mL) and 0.4 mL of PG-25K (2.5 mg/mL), respectively.

2.6. UV−Vis and Fourier Transform Infrared Spectroscopic Studies of Nanoparticles. The absorption spectrum was recorded using a Cary 4000 UV−vis spectrophotometer. FTIR spectroscopy was performed using a PerkinElmer FTIR Spectra 100 spectrometer fitted with a diamond ATR. The nanoparticles samples were first dried on the ATR crystal, and spectra were acquired at 400−4000 cm^{-1} wavenumbers with a 4 cm^{-1} resolution. The spectra were further analyzed by Origin 7.0 software.

2.7. Size Measurement with Dynamic Light Scattering. AgNPs were characterized in terms of sizes using dynamic light scattering with a commercial Zetasizer (Malvern Zetasizer Nano ZS, Malvern Instruments). For size measurements the instrument was calibrated using a 60 nm polystyrene standard. We loaded samples into disposable cells, and particle size measurements were done in duplicate.

2.8. Electron Microscopy. Transmission electron microscopy (TEM) images were collected with a Hitachi H-7500 transmission electron microscope (Hitachi High Technologies American, Pleasanton, CA) equipped with a Gatan BioScan CCD camera (Gatan Inc., Pleasanton, CA) operating at an acceleration voltage of 75 kV. Nanoparticle samples were prepared in DI water and were centrifuged

dx.doi.org/10.1021/la305068p | Langmuir 2013, 29, 4225−4234

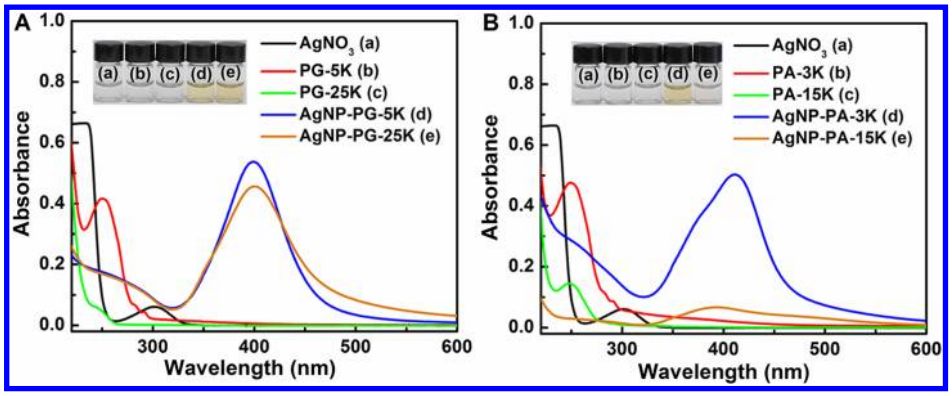

Figure 2. (A) UV−vis spectra of (a) 10 mM $AgNO_3$ (black line), (b) aqueous PG-5K (red line), (c) aqueous PG-25K (green line), (d) AgNP-PG-5K (blue line), and (e) AgNP-PG-25K (orange line). (B) UV−vis spectra of (a) 10 mM $AgNO_3$ (black line), (b) aqueous PA-3K (red line), (c) aqueous PA-15K (green line), (d) AgNP-PA-3K (blue line), and (e) AgNP-PA-15K (orange line). Corresponding photographs of these solutions are shown in the inset.

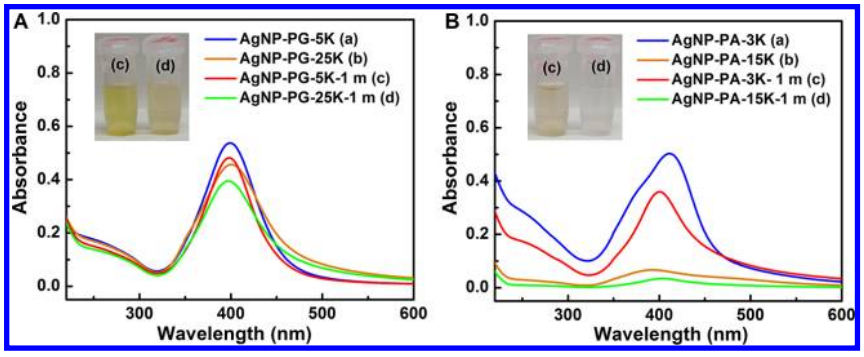

Figure 3. (A) UV−vis spectra of (a) AgNP-PG-5K (blue line), (b) AgNP-PG-25K (orange line), a month old solution of (c) AgNP-PG-5K-1m (red line), and a month old solution of (d) AgNP-PG-25K-1m (green line). (B) UV−vis spectra of (a) AgNP-PA-3K (blue line), (b) AgNP-PA-15K (orange line), a month old solution of (c) AgNP-PA-3K-1m (red line), and a month old solution of (d) AgNP-PA-15K-1m (green line). Photographs of month old solutions are shown in the inset.

and redispersed in DI water. These solutions were filtered through 200 nm syringe filters before applying on grids for TEM measurements. Samples were prepared by spreading a 5.0 μL of sample on an ultrathin 300 mesh Formvar/carbon-coated copper grid and dried in air.

2.9. Catalytic Study. The catalytic reduction reaction of 4-nitrophenol was performed in aqueous solution in a standard quartz cell with a 1 cm path length. The reaction procedure was as follows: 0.12 mL of 0.1 M $NaBH_4$ was mixed with 24 μL of 5.0 mM 4-nitrophenol in a 1.5 mL Eppendorf tube, and the volume was adjusted to 1.0 mL with deionized water (DI). The overall concentrations of 4-nitrophenol and $NaBH_4$ were 0.12 and 12 mM, respectively. That lead to a color change from light yellow to yellow-green. The solution was transferred to a standard quartz cell (0.7 mL) for UV−vis measurements. For those samples with silver nanoparticles, 24 μL of 5.0 mM 4-nitrophenol and 25 μL of AgNP-PG-5K were mixed in a 1.5 mL Eppendorf tube, and then 0.12 mL of 0.1 M $NaBH_4$ was added before adjusting the volume to 1.0 mL. Immediately after that, the solution was transferred to a standard quartz cell, and the UV−vis absorption spectra were recorded with a time interval of 80 s in a scanning range of 200−700 nm at ambient temperature (25 ± 2 °C).

3. RESULTS AND DISCUSSION

Four different polymer-stabilized silver nanoparticles (AgNPs), AgNP-PG-5K, AgNP-PG-25K, AgNP-PA-3K, and AgNP-PA-15K, were simply synthesized by reducing silver ion in aqueous solutions of the polymer as discussed in the Experimental Section. The physicochemical properties of the samples such as stability, size, morphology, and chemical activty were characterized.

3.1. Characterization of AgNPs by UV−vis Spectroscopy. UV−vis spectra of the AgNPs are presented in Figure 2A,B, and it is evident that metallic AgNPs were formed. The absorbance maximum observed at 392−420 nm is characteristic of silver surface plasmon resonance (SPR).[42] Figure 2 shows the UV−vis spectra of the silver nanoparticles prepared with different polymers at the same $AgNO_3$ concentrations. For comparison, the UV−vis spectra of $AgNO_3$ and the polymer alone are presented along with their nanoparticles solutions. Figure 2A shows the UV−vis spectra of 10 mM $AgNO_3$ (curve a), aqueous PG-5K (curve b), aqueous PG-25K (curve c), colloidal AgNP-PG-5K (curve d), and colloidal AgNP-PG-25K (curve e). In Figure 2A (curve a), there is only one signal at 301 nm characteristic of silver ion (Ag^+) in aqueous solution; in curve b, the signal at 250 nm is characteristic of PG-5K in aqueous solution, and in curve c, the signal at 250 nm is characteristic of PG-25K. For curves d and e there is only a dominant absorption maximum at 399 nm (absorbance 0.54) and 400 nm (absorbance 0.46), respectively, characteristic of colloidal AgNPs. This is indicative of AgNP-PG-5K (curve d) and AgNP-PG-25K (curve e) nanoparticles being formed. The dispersity of AgNPs was evaluated by comparing the full width at half-maximum (fwhm)[43] from the UV−vis spectra. The fwhm of colloidal AgNP-PG-5K and AgNP-PG-25K are 65 ± 1 and 80 ± 2 nm, respectively. This indicates that AgNP-PG-5K was relatively monodispersed and AgNP-PG-25K was relatively polydispersed.[43] Figure 2B show data for studies with the PA samples. Curve a is for silver ion (Ag^+) in aqueous solution,

dx.doi.org/10.1021/la305068p | Langmuir 2013, 29, 4225−4234

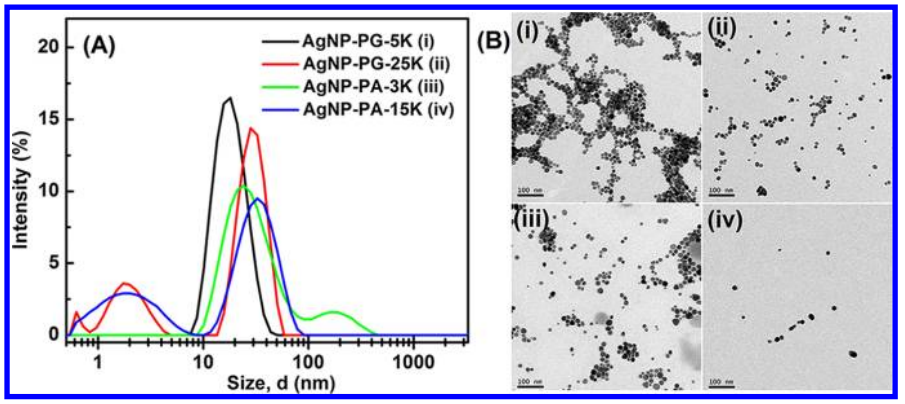

Figure 4. (A) Hydrodynamic diameter of (i) AgNP-PG-5K (black line), (ii) AgNP-PG-25K (red line), (iii) AgNP-PA-3K (green line), and (iv) AgNP-PA-15K (blue line). (B) TEM images of (i) AgNP-PG-5K, (ii) AgNP-PG-25K, (iii) AgNP-PA-3K, and (iv) AgNP-PA-15K conjugates. Images were taken with a Hitachi H-7500 transmission electron microscope at an accelerating voltage of 75 kV. Samples were prepared by spreading 5 μL of aqueous sample on an ultrathin 300 mesh Formvar/carbon film on copper grid and dried in air.

curve b is for PA-3K in aqueous solution with a characteristic signal at 250 nm, and curve c is for PA-1K in aqueous solution with a characteristic signal at 248 nm. For curve d there is one dominant absorption maximum at 410 nm (absorbance 0.50) characteristic of the colloidal AgNPs. The fwhm of colloidal AgNP-PA-3K is 85 ± 2. This indicates that the sample was relatively polydispersed.[43] For curve e, the absorption maximum is at 393 nm (absorbance 0.07) with an additional shoulder at 485 nm. There is no evidence of the presence of Ag^+ ions in solution from the spectrum (curve e). However, the fwhm of colloidal AgNP-PA-15K is 130 ± 3. This is indicative of the fact the AgNP-PA-15K (curve e) is relatively polydispersed.[44] The digital pictures of all the solutions were presented in the inset of Figure 2A.

UV−vis spectra shown in Figure 3 demonstrate the stability of colloidal nanoparticles in aqueous solutions. Colloidal AgNPs have inherent tendency to oxidize in the presence of oxygen making them less attractive from the point of view of stability and shelf life.[45] The stability of colloidal AgNPs were monitored for a month. In the presence of the PG polymers AgNPs were moderately stable compared to PA-3K and PA-15K. In Figure 3A, the UV−vis spectra of AgNP-PG-5K (curve a), AgNP-PG-25K (curve b), AgNP-PG-5K-1m (curve c, sample a after 1 month), and AgNP-PG-25K-1m (curve d, sample in curve b after 1 month) are shown. Absorption maximum of AgNP-PG-5K (curve a) at 399 nm (absorbance 0.54) changes to 398 nm (absorbance 0.48) (curve c) after a month. In addition, the fwhm of colloidal AgNP-PG-5K changes from 65 ± 1 to 61 ± 1 nm after a month. Absorption maximum of AgNP-PG-25K (curve b) at 400 nm (absorbance 0.46) changes to 398 nm (absorbance 0.39) (curve d) after a month. In addition, the fwhm of colloidal AgNP-PG-25K changes from 80 ± 2 to 75 ± 1 nm after a month. The decrease in absorbance is about 0.06 units, and the shift in absorption position is not more than 2 nm in both cases. These slight changes indicate that some of the surface silver atoms are oxidized over the course of 1 month,[46,47] but there is minimal size decrease and the AgNPs essentially remain relatively monodispersed. In Figure 3B, the UV−vis spectra of AgNP-PA-3K (curve a), AgNP-PA-15K (curve b), AgNP-PA-3K-1m (curve c, sample a after 1 month), and AgNP-PA-15K-1m (curve d, sample in curve b after 1 month) are shown. Absorption maximum of AgNP-PA-3K (curve a) at 410 nm (absorbance 0.50) changes to 400 nm (absorbance 0.36) (curve c) after a month. In addition, the fwhm of colloidal AgNP-PA-3K changes from 85 ± 2 to 73 ± 1 nm after a month. The decrease in absorbance is 0.14 units, and the shift in absorption position is 10 nm. These larger shifts indicate that surface silver atoms are oxidized significantly over the course of 1 month.[46,47] However, AgNP-PA-3K essentially remains relatively polydispersed. The absorption maximum of AgNP-PA-15K (curve b) at 393 nm (absorbance 0.07) changes to 403 nm (absorbance 0.034) (curve d), and the shoulder at 485 nm disappears after a month. In addition, the fwhm of colloidal AgNP-PA-15K changes from 130 ± 3 to 74 ± 1 nm after a month. This change indicates that in the course of a month the large aggregates were dispersed to relatively larger AgNPs, and some surface silver atoms are also lost as Ag^+ ions due to oxidation.[46,47] It is worthwhile to mention here that we do not observe any absorption maximum for the dissociated silver ions (Ag^+) in Figure 3 as they are under the detection limit. In Figure 2 it was shown that the absorption maximum of 10 mM silver ion has a absorbance of 0.06. During the synthesis of AgNPs we have used overall 10 mM of $AgNO_3$, and the solution was allowed to stand overnight to allow all the Ag^+ ions to reduce to elemental silver atoms. In addition, we have performed centrifugal purification to get rid of unreduced Ag^+ ions. Hence, due to the oxidation of the AgNPs after 1 month, the solutions are not producing enough silver ion to be detectable by UV−vis spectroscopy.

3.2. Dynamic Light Scattering Size Data and TEM Images. Dynamic light scattering (DLS) and transmission electron microscopy (TEM) were employed to analyze the size and morphology of AgNPs. Dynamic light scattering (DLS) is the most versatile and useful set of techniques for measuring *in situ* the sizes, size distributions, and (in some cases) the shapes of nanoparticles in liquids.[48] As shown in Figure 4A, the hydrodynamic diameter of AgNP-PG-5K was equal to 18 ± 1 nm (polydispersity index, PDI 0.090) (black line). The polydispersity index is dimensionless and scaled such that values smaller than 0.05 are rarely seen other than with highly monodisperse samples. A polydispersity index of 0.1 is suggested as a suitable limit of monodispersity and values greater than 0.7 indicate that the sample has a very broad size distribution.[49] The corresponding TEM image in Figure 4B (i) supports this size distribution for AgNP-PG-5K. In Figure 4A three populations of the AgNP-PG-25K (red line) were found to be located in 0.6 nm (at 2% intensity), 2.0 nm (at 23%

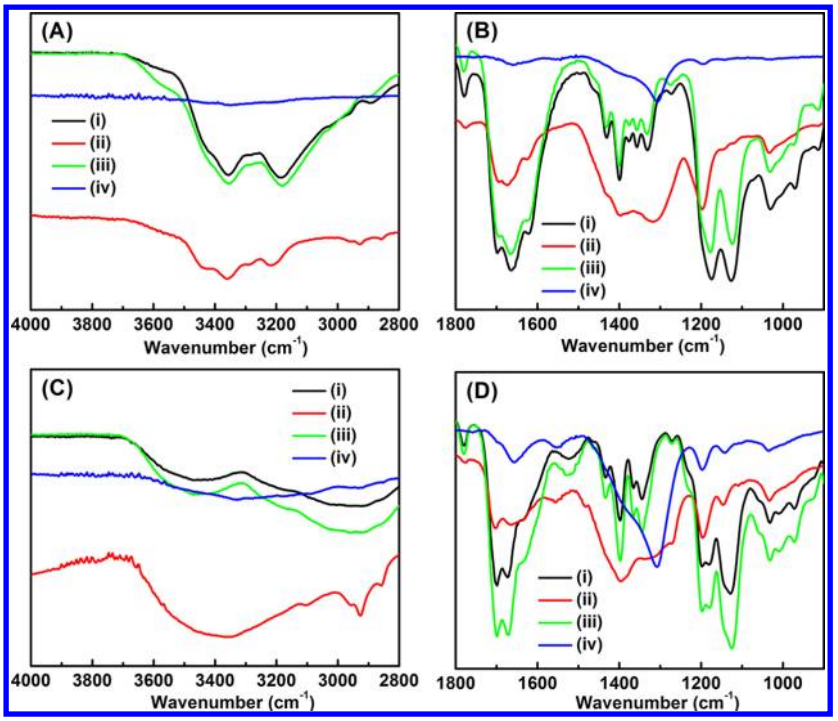

Figure 5. (A, B) FTIR spectra of (i) solid PG-5K (black line), (ii) AgNP-PG-5K conjugates (red line), (iii) solid PG-25 (green line), and (iv) AgNP-PG-25K (blue line) conjugates. (C, D) FTIR spectra of (i) solid PA-3K (black line), (ii) AgNg-PA-3K conjugates (red line), (iii) solid PA-15 (green line), and (iv) AgNP-PA-15K (blue line) conjugates.

intensity), and 30 nm (75% intensity) with a PDI of 0.175. The TEM image in Figure 4B (ii) supports these distribution. In Figure 4A two populations were found for AgNP-PA-3K (green line) in 30 nm (at 88% intensity) and 158 nm (at 12% intensity) with a PDI of 0.339. Similarly, two populations were found for AgNP-PA-15K (blue line) in 35 nm (at 68% intensity) and 2.0 nm (at 32% intensity) with a PDI of 0.090. The TEM images in Figure 4B (iii) and (iv) support these distributions. The TEM images of 1 month old samples are given in Figure S2 (Supporting Information). UV−vis spectroscopy is widely used to characterize silver nanoparticles. The surface plasmon resonance (SPR) band corresponds to the AgNPs size, and the red-shift in the SPR band qualitatively indicates an increase in AgNPs size.[50] The absorption maxima of 399 nm for AgNP-PG-5K (Figure 2A) indicates the presence of roughly spherical AgNPs, and the corresponding DLS signal (Figure 4A) displays a size of 18 ± 1 nm (PDI 0.090). Previous literature reports indicate that an SPR band of 402 nm corresponds to a diameter of ∼21 nm AgNPs.[50] Thus, UV−vis absorption maximum of AgNP-PG-5K provide qualitative size distributions. However, the TEM image for the dried samples show agglomerates of small grains and some dispersed nanoparticles (Figure 4B (i)). In contrast, the other three sets of AgNPs reported here have two size distributions with wide polydispersity as indicated by DLS and therefore do not follow a clear trend corresponding to the SPR absorption maxima.

3.3. Characterization of AgNPs by FTIR Spectroscopy.

The changes in specific stretching and bending vibrations of molecules due to conjugation with nanoparticles can be observed by FTIR spectroscopy.[51,52] The FTIR spectra of polymer used in this study comprise of several bands as shown in Figure 5, and their assignment are presented in Table 1. The characteristic signals responsible for the polymer−AgNPs interaction are C−N stretching (alkyl), N−H stretching, C−N stretching (aryl), and C═O stretching. The band at 1177 cm^{-1} in PG-5K is due to C−N stretching vibration of guanidino group and this band shift to 1198 cm^{-1} in AgNP-PG-5K (Figure 5B). Only two N−H stretching vibrations of guanidino group appear at 3189 and 3364 cm^{-1} in PG-5K. In the corresponding AgNP-PG-5K conjugates there are three distinct N−H signals are seen at 3216, 3359, and 3437 cm^{-1} (Figure 5A). The band at 1273 cm^{-1} in PG-5K is due to C−N stretching vibration of cyclic amido group and this band shift to 1319 cm^{-1} in AgNP-PG-5K (Figure 5B). The C═O stretching vibrations of cyclic amido group appears at 1665 cm^{-1} in PG-5K. In the corresponding AgNP-PG-5K conjugates this signals appears at 1675 cm^{-1} (Figure 5B). The observed shifts, especially in guanidino C−N and N−H stretches, are indicative of the fact that PG-5K binds to the AgNPs surface facing the guanidino group.[51,52] For PG-25K the signals are C−N stretching vibration at 1180 cm^{-1} (Figure 5B), N−H stretching

Table 1. Vibrational Band Assignment in FTIR Spectra of Polymer and Polymer Bound AgNPs

sample	ν_{C-N} (alkyl, cm^{-1})	ν_{N-H} (cm^{-1})	ν_{C-N} (cyclic, cm^{-1})	$\nu_{C=O}$ (cm^{-1})
PG-5K	1177	3189, 3364	1273	1665
AgNP-PG-5K	1198	3216, 3359, 3437	1319	1675
PG-25K	1180	3183, 3357	1275	1665
AgNP-PG-25K	1198	3340	1308	1658
PA-3K	1129	3448	1273	1675, 1698
AgNP-PA-3K	1147	3400	1317	1667, 1704
PA-15K	1125	3367	1273	1673, 1700
AgNP-PA-15K	1143	3333	1308	1657

dx.doi.org/10.1021/la305068p | Langmuir 2013, 29, 4225−4234

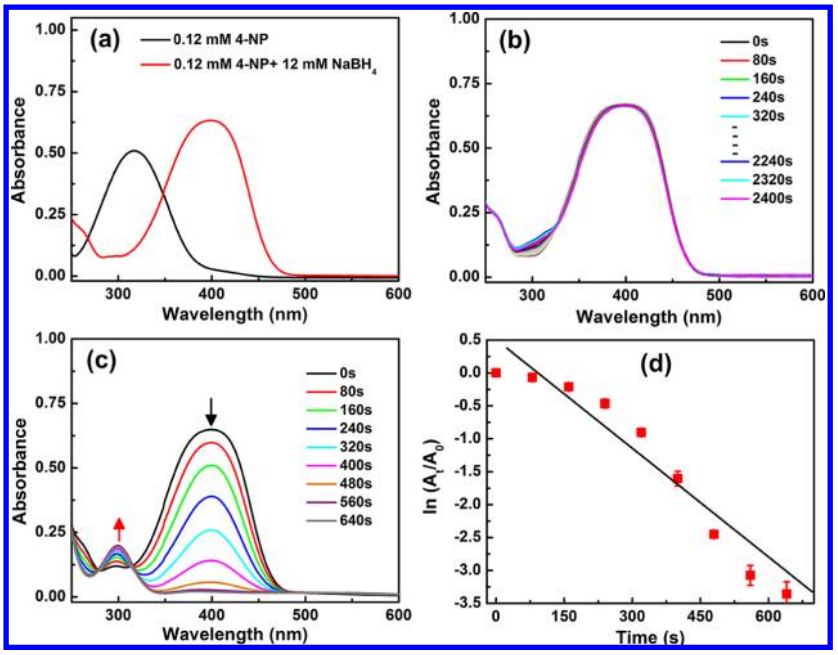

Figure 6. UV−vis spectra of 0.12 mM 4-nitrophenol (4-NP) (black line) and 0.12 mM 4-nitrophenol with 12 mM $NaBH_4$ (red line) (a); 0.12 mM 4-nitrophenol with 12 mM $NaBH_4$ without addition of any catalyst (b); 0.12 mM 4-nitrophenol with 12 mM $NaBH_4$ in the presence of AgNP-PG-5K as catalyst (c) and plot of $\ln(A_t/A_0)$ against the reaction time for pseudo-first-order reduction kinetics of 4-nitrophenol in the presence of excess $NaBH_4$ (12 mM) in aqueous solutions (d).

vibrations at 3183 and 3357 cm^{-1} (Figure 5A), C−N stretching vibration at 1275 cm^{-1} (Figure 5B), and C═O stretching vibration at 1665 cm^{-1} (Figure 5B). In AgNP-PG-25 the corresponding signals are C−N stretching vibration at 1198 cm^{-1} (Figure 5B), N−H stretching vibrations at 3340 cm^{-1} (Figure 5A), C−N stretching vibration at 1308 cm^{-1} (Figure 5B), and C═O stretching vibration at 1658 cm^{-1} (Figure 5B). These change in the FTIR signals of PG-25 while bound to the AgNPs account for the interaction of the polymer with AgNPs.[51,52]

Similarly, the band at 1129 cm^{-1} in PA-3K is due to the C−N stretching vibration of the amino group and this band shifts to 1147 cm^{-1} in AgNP-PA-3K (Figure 5D). Only one broad N−H stretching vibration of amino group appears at 3448 cm^{-1} in PA-3K. In the corresponding AgNP-PA-3K conjugates there is a distinct N−H signal at 3400 cm^{-1} (Figure 5C). The band at 1273 cm^{-1} in PA-3K is due to the C−N stretching vibration of the cyclic amido group and this band shifts to 1317 cm^{-1} in AgNP-PA-3K (Figure 5D). The C═O stretching vibrations of the cyclic amido group appears at 1675 and 1698 cm^{-1} in PA-3K. In the corresponding AgNP-PA-3K conjugates these signals appear at 1667 and 1704 cm^{-1} (Figure 5D). The observed shifts, especially in the amido C−N and N−H stretches, is indicative of the fact that PA-3K binds to the AgNPs surface facing the amido group.[51,52] For PA-15K the signals are the C−N stretching vibration at 1125 cm^{-1} (Figure 5D), N−H stretching vibrations at 3367 cm^{-1} (Figure 5C), C−N stretching vibration at 1273 cm^{-1} (Figure 5D), and C═O stretching vibration at 1673 and 1700 cm^{-1} (Figure 5D). In AgNP-PA-15 the corresponding signals are the C−N stretching vibration at 1143 cm^{-1} (Figure 5D), N−H stretching vibrations at 3333 cm^{-1} (Figure 5C), C−N stretching vibration at 1308 cm^{-1} (Figure 5D), and C═O stretching vibration at 1657 cm^{-1} (Figure 5B). These changes in the FTIR signals of PA-15 are due to the complexation with the nanoparticles' surface.[53]

3.4. Application of AgNP-PG-5K for Catalytic Reduction of 4-Nitrophenol. A potential application of metal nanoparticles is the catalysis of certain reactions that would otherwise not occur. In this report we have chosen the reduction of 4-nitrophenol to 4-aminophenol as a model system[40,41] in order to evaluate the catalytic activity of AgNP-PG-5K. The reduction of 4-nitrophenol ($E^0_{(4\text{-NP/4-AP})} = -0.76$ V) by sodium borohydride ($NaBH_4$) ($E^0_{(H_3BO_3/BH_4^-)} = -1.33$ V) is thermodynamically feasible but kinetically restricted in the absence of a catalyst. Addition of $NaBH_4$ to a 4-nitrophenol solution changes the light yellow color of the solution to intense yellow due to formation of the 4-nitrophenolate ion.[40] This is due to the fact that addition of $NaBH_4$ changes the pH from acidic to highly basic. Accordingly, the absorption peak shifts from 317 to 400 nm (Figure 6a). The catalytic process of this reaction was monitored by UV−vis spectroscopy, as illustrated in Figure 6. Absorption intensity at 400 nm for the 4-nitrophenolate ion remained unaltered in the presence of only $NaBH_4$ even after 40 min (2400 s) as shown in Figure 6b. This result indicated that the reduction does not proceed without a catalyst. Figure 6c illustrates the reduction reaction of 4-nitrophenol, observed at different time intervals using AgNP-PG-5K as the catalyst. According to our DLS and TEM data (Figure 4) AgNP-PG-5K is relatively monodispersed, and thus we have chosen AgNP-PG-5K to explore catalytic activity. Silver nanoparticles though also absorb around 400 nm. In order to avoid the overlap between the SPR band of AgNP-PG-5K and 4-nitrophenol, only 25 μL of AgNP-PG-5K was used in a total of 1.0 mL volume to monitor the catalytic action. Absorbance of 25 μL of AgNP-PG-5K is only 0.04 as illustrated in Figure S1 (Supporting Information). In the presence of AgNP-PG-5K and $NaBH_4$ the 4-nitrophenol was reduced, and the intensity of the absorption peak at 400 nm gradually decreased with time and after ∼10 min it fully disappeared (Figure 6c). In the meantime, a new absorption peak appeared

dx.doi.org/10.1021/la305068p | Langmuir 2013, 29, 4225−4234

at 298 nm and progressively increased in intensity (Figure 6c). This new peak is attributed to the typical absorption of 4-aminophenol. The UV−vis spectra in Figure 6c showed two isosbestic points at 280 and 314 nm. This result suggests that the catalytic reduction of 4-nitrophenol exclusively yielded 4-aminophenol, without any other side products.[54]

In the reduction process, the overall concentration of $NaBH_4$ was 12 mM and 4-nitrophenol was 0.12 mM. Considering the much higher concentration of $NaBH_4$ compared to that of 4-nitrophenol, the pseudo-first-order kinetics could be applied with respect to 4-nitrophenol in order to determine the catalytic activity of AgNP-PG-5K. The absorbance of 4-nitrophenol is proportional to its concentration in solution; the absorbance at time t (A_t) and time $t = 0$ (A_0) are equivalent to the concentration at time t (C_t) and time $t = 0$ (C_0). The rate constant (k) was determined from the linear plot of $\ln(A_t/A_0)$ versus reduction time in seconds, and the constant was estimated to be 5.50×10^{-3} s^{-1} (Figure 6d). In order to compare the catalytic activity of current catalyst with the ones reported in the literature with AgNP, it is not entirely appropriate to compare the rate constant. Hence, the activity parameter $\kappa = k/m$—which is the ratio of rate constant k to the total mass of the catalyst added—was used to estimate the catalytic performance of the catalyst.[54,55] The reported activity parameters reported by Rashid et al.[56] are 1.30, 0.41, and 0.09 s^{-1} g^{-1} for coral-like dendrite, banana leave-like dendrite, and spherical Ag nanostructures. Tang and co-workers[3] designed AgNP/C nanocomposites having an activity parameter of 1.69 s^{-1} g^{-1}. Core−shell nanocomposite, Fe_3O_4-@SiO_2-Ag reported by Chi et al.[55] and Shin et al.[57] have an activity parameter of 7.67 and 275 s^{-1} g^{-1}, respectively. Very recently, An and co-workers reported microspheres of Fe_3O_4-@C@Ag with an activity parameter 372 s^{-1} g^{-1}. All these activity parameters containing nanostructured silver are lower than the 1375 s^{-1} g^{-1} of AgNP-PG-5K nanoparticles synthesized in this work. However, this value is comparable to the core−shell microspheres, Fe_3O_4-@SiO_2-Ag-Au, containing additional gold layer as reported by An and co-workers.[54] All these parameters are summarized in Table 2. It is worthwhile to mention at this context that gold nanoparticles have also served as catalysts for the reduction of 4-nitrophenol. A recent study by Zhang et al.[58] reported the activity parameter, κ, for AuNP-based catalysis and summarized several other AuNP−polymer-based catalysts.[58] All of these have a lower κ value than the AgNP-PG-5K conjugates reported here. The good catalytic activity of AgNP-PG-5K nanoparticles is attributed to the fact that these particles are well monodispersed in solution and their relatively smaller size (~18 nm). The smaller size consists of a high surface-to-volume ratio and more exposed Ag atoms on the surface, and these exposed atoms potently act as the catalytic sites.[55] These results suggested that AgNP-PG-5K might possess an important application in the field of heterogeneous catalysis.

Table 2. Summary of the Activity Parameter, κ, Dependent on the Rate Constants of the Reaction (k) and the Amounts of Catalyst Used

nanoparticles	catalyst (mg)	k (s^{-1})	κ (s^{-1} g^{-1})	ref
TAC-Ag-1.0	4.0	5.19×10^{-3}	1.30	56
TAC-Ag-1.4	4.0	1.65×10^{-3}	0.41	56
TSC-Ag-1.4	4.0	3.64×10^{-4}	0.09	56
Ag-NP/C composite	1.0	1.69×10^{-3}	1.69	3
Fe_3O_4-@SiO_2-Ag	1.0	7.67×10^{-3}	7.67	55
Fe_3O_4/SiO_2-Ag	0.02	5.50×10^{-3}	275	57
Fe_3O_4-@C@Ag	0.01	3.72×10^{-3}	372	54
Fe_3O_4-@C@Ag-Au	0.01	15.80×10^{-3}	1580	54
AgNP-PG-5K	0.004	5.50×10^{-3}	1375	this work

3.5. Mechanism of Reduction of 4-Nitrophenol to 4-Aminophenol by $NaBH_4$. Recently, the reaction of sodium borohydride with metal surfaces and its decomposition in presence of metal nanoparticles is an interesting area of research due to its potential application in fuel cells.[59,60] The mechanism of reduction of 4-nitrophenol to 4-aminophenol by $NaBH_4$ in the presence of silver nanoparticles is discussed in terms of the Langmuir−Hinshelwood (LH) model[59,61] illustrated in Figure 7. Borohydride ions adsorb on the surface of the AgNP nanoparticles and transfer a surface-hydrogen species to the surface of the nanoparticles.[59,62] This reversible step can be modeled in terms of a Langmuir isotherm.[59] Concomitantly, 4-nitrophenol molecules are adsorbed on the surface of the nanoparticles. This reversible process can also be modeled by a Langmuir isotherm.[59] Moreover, the adsorption/desorption equilibriums and diffusion of reactants to the nanoparticles are considered to be fast.[59] The reduction of 4-nitrophenol, which is the rate-determining step, occurs due to the reaction of adsorbed 4-nitrophenol with the nanoparticles surface-bound hydrogen atoms (Figure 7).[59] When product, 4-aminophenol, desorbs leaving free metal surface, the catalytic cycle can begin again.[59]

4. CONCLUSIONS

Four different colloidal silver nanoparticles, namely AgNP-PG-5K, AgNP-PG-25K, AgNP-PA-3K, and AgNP-PA-15K, were prepared *in situ* by reducing the Ag^+ ions in solutions of polyamino and polyguanidino oxonorbornenes with sodium borohydride ($NaBH_4$). Very recently, Lin and co-workers reported[63] a AgNP−nanosilicate platelate hybrid, and these were further blended with water-soluble poly(ether)urethane (PEU). These conjugates promoted antimicrobial activity as well as reduce the inflammatory response.[63] Santos et al.[64] introduced new AgNP conjugates stabilized by linear polyethylenimine (LPEI). They systematically modified the LPEI framework to create new ligands of polymer stabilizers. They also tested the catalytic activity in the reduction reaction of 4-nitrophenol, and their kinetics were fully analyzed.[64] In another very recent study by again Lin and co-workers,[65] they emphasized the importance of the existence of polymeric coatings on both AgNPs surfaces and the surfaces they interact with in stabilizing nanoparticles against deposition. This study suggested that although polymeric coatings are stabilizers of AgNPs, they might stabilize AgNPs against deposition unless the collector surface is also polymer coated.[65] Polymers reported in this work stabilize AgNPs and kept them in aqueous solutions for more than a month. To our knowledge, this is the first report of stabilizing colloidal silver nanoparticles by cationic polynorbornenes. Compared with the amino polymers (PA-3K and PA-15K), the guanidino analogues (PG-5K and PG-25) better stabilized the silver colloids as evident from the spectroscopic data. Also, there seems to be a polymer size dependence on stability with the shorter PG (PG-5K) being more effective than the longer PG (PG-25K). The catalytic activity of AgNP-PG-5K nanoparticles thus prepared was investigated in the reduction reaction of 4-nitrophenol to 4-aminophenol by $NaBH_4$. A comparative study revealed that the

dx.doi.org/10.1021/la305068p | Langmuir 2013, 29, 4225−4234

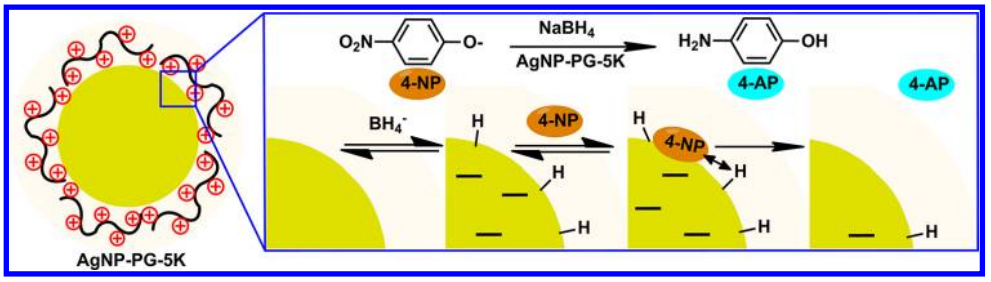

Figure 7. Langmuir–Hinshelwood (LH) model for the mechanism of the reduction of 4-nitrophenol (4-NP) to 4-aminophenol (4-AP) by $NaBH_4$ in the presence of metallic nanoparticles. The AgNP-PG-5K nanoparticles react with borohydride (BH_4^-) ions to form the silver hydride. At the same time 4-nitrophenol adsorbs on to the silver surface and adsorption/desorption of both the reagents on the surface is fast following Langmuir isotherm. The rate-determining step is the reduction of the adsorbed 4-nitrophenol to 4-aminophenol, and the later desorbs right after formation.

activity parameters, κ, of the nanoparticles synthesized in this work are better than nanocomposites and microspheres with embedded AgNPs reported in the literature. These nanoparticles could be very useful in catalytic applications. Furthermore, the polymers PG and PA being biocompatible, polymer-bound silver nanoparticles could be integrated into various biomedical and biosensor applications and worth studying in the future.

■ ASSOCIATED CONTENT

Supporting Information

Additional UV–vis spectral data, TEM images of 1 month old silver nanoparticles, and table that summarizes the activity parameter κ (s^{-1} g^{-1}) of gold nanoparticles from the literature. This material is available free of charge via the Internet at http://pubs.acs.org.

■ AUTHOR INFORMATION

Corresponding Author

*Tel +1 678 797 2654, +1 678 797 2653; fax + 1 770 423 6744; e-mail bbaruah@kennesaw.edu (B.B.), ggabrie2@kennesaw.edu (G.J.G.).

Notes

The authors declare no competing financial interest.

■ ACKNOWLEDGMENTS

This work was supported by start-up funds from the Chemistry and Biochemistry, Kennesaw State University, and KSU CSM Mentor Protégé funds (BARUAH-05-FY2011-02 and GGAB-RI-08-FY2010-11). B.B. and G.G. also thank Dr. Mark Mitchell, Department Chair, and Dr. Ronald Matson, Dean of the College of Science and Mathematics, for their enormous support. We acknowledge the Robert P. Apkarian Integrated Electron Microscopy Core of Emory University for use of its Electron Microscopy facility. B.B. and G.G. are thankful to Dr. David Gottfried at Georgia Institute of Technology, NRC, for dynamic light scattering experiments.

■ REFERENCES

(1) El-Sayed, M. A. Some Interesting Properties of Metals Confined in Time and Nanometer Space of Different Shapes. *Acc. Chem. Res.* **2001**, *34*, 257–264.

(2) Wang, L.; Luo, J.; Shan, S.; Crew, E.; Yin, J.; Zhong, C.-J.; Wallek, B.; Wong, S. S. S. Bacterial Inactivation Using Silver-Coated Magnetic Nanoparticles as Functional Antimicrobial Agents. *Anal. Chem.* **2011**, *83*, 8688–8695.

(3) Tang, S.; Vongehr, S.; Meng, X. Carbon Spheres with Controllable Silver Nanoparticle Doping. *J. Phys. Chem. C* **2010**, *114*, 977–982.

(4) Yamamoto, M.; Kashiwagi, Y.; Nakamoto, M. Size-Controlled Synthesis of Monodispersed Silver Nanoparticles Capped by Long-Chain Alkyl Carboxylates from Silver Carboxylate and Tertiary Amine. *Langmuir* **2006**, *22*, 8581–8586.

(5) Kim, J.-Y.; Lee, J.-S. Synthesis and Thermodynamically Controlled Anisotropic Assembly of DNA-Silver Nanoprism Conjugates for Diagnostic Applications. *Chem. Mater.* **2010**, *22*, 6684–6691.

(6) Zhang, Q.; Li, W.; Moran, C.; Zeng, J.; Chen, J.; Wen, L.-P.; Xia, Y. Seed-Mediated Synthesis of Ag Nanocubes with Controllable Edge Lengths in the Range of 30–200 nm and Comparison of Their Optical Properties. *J. Am. Chem. Soc.* **2010**, *132*, 11372–11378.

(7) Netzer, N. L.; Gunawidjaja, R.; Hiemstra, M.; Zhang, Q.; Tsukruk, V. V.; Jiang, C. Formation and Optical Properties of Compression-Induced Nanoscale Buckles on Silver Nanowires. *ACS Nano* **2009**, *3*, 1795–1802.

(8) Tang, B.; An, J.; Zheng, X.; Xu, S.; Li, D.; Zhou, J.; Zhao, B.; Xu, W. Silver Nanodisks with Tunable Size by Heat Aging. *J. Phys. Chem. C* **2008**, *112*, 18361–18367.

(9) Halvorson, R. A.; Vikesland, P. J. Surface-Enhanced Raman Spectroscopy (SERS) for Environmental Analyses. *Environ. Sci. Technol.* **2010**, *44*, 7749–7755.

(10) Shon, Y.-S.; Cutler, E. Aqueous Synthesis of Alkanethiolate-Protected Ag Nanoparticles Using Bunte Salts. *Langmuir* **2004**, *20*, 6626–6630.

(11) Jana, N. R.; Peng, X. Single-Phase and Gram-Scale Routes toward Nearly Monodisperse Au and Other Noble Metal Nanocrystals. *J. Am. Chem. Soc.* **2003**, *125*, 14280–14281.

(12) Tan, S.; Erol, M.; Attygalle, A.; Du, H.; Sukhishvili, S. Synthesis of Positively Charged Silver Nanoparticles via Photoreduction of $AgNO_3$ in Branched Polyethyleneimine/HEPES Solutions. *Langmuir* **2007**, *23*, 9836–9843.

(13) Zhu, Y.; Qian, Y.; Li, X.; Zhang, M. [gamma]-Radiation Synthesis and Characterization of Polyacrylamide-Silver Nanocomposites. *Chem. Commun.* **1997**, 1081–1082.

(14) Jiang, L.-P.; Xu, S.; Zhu, J.-M.; Zhang, J.-R.; Zhu, J.-J.; Chen, H.-Y. Ultrasonic-Assisted Synthesis of Monodisperse Single-Crystalline Silver Nanoplates and Gold Nanorings. *Inorg. Chem.* **2004**, *43*, 5877–5883.

(15) Hu, B.; Wang, S.-B.; Wang, K.; Zhang, M.; Yu, S.-H. Microwave-Assisted Rapid Facile "Green" Synthesis of Uniform Silver Nanoparticles: Self-Assembly into Multilayered Films and Their Optical Properties. *J. Phys. Chem. C* **2008**, *112*, 11169–11174.

(16) Tan, Y.; Li, Y.; Zhu, D. Preparation of Silver Nanocrystals in the Presence of Aniline. *J. Colloid Interface Sci.* **2003**, *258*, 244–251.

(17) Yu, D.; Yam, V. W.-W. Controlled Synthesis of Monodisperse Silver Nanocubes in Water. *J. Am. Chem. Soc.* **2004**, *126*, 13200–13201.

(18) Giersig, M.; Pastoriza-Santos, I.; Liz-Marzan, L. M. Evidence of an Aggregative Mechanism during the Formation of Silver Nanowires in N,N-Dimethylformamide. *J. Mater. Chem.* **2004**, *14*, 607–610.

(19) Tan, Y.; Dai, X.; Li, Y.; Zhu, D. Preparation of Gold, Platinum, Palladium and Silver Nanoparticles by the Reduction of Their Salts

with a Weak Reductant-Potassium Bitartrate. *J. Mater. Chem.* **2003**, *13*, 1069−1075.
(20) Lee, G.-J.; Shin, S.-I.; Kim, Y.-C.; Oh, S.-G. Preparation of Silver Nanorods through the Control of Temperature and pH of Reaction Medium. *Mater. Chem. Phys.* **2004**, *84*, 197−204.
(21) Sun, Y.; Yin, Y.; Mayers, B. T.; Herricks, T.; Xia, Y. Uniform Silver Nanowires Synthesis by Reducing $AgNO_3$ with Ethylene Glycol in the Presence of Seeds and Poly(Vinyl Pyrrolidone). *Chem. Mater.* **2002**, *14*, 4736−4745.
(22) Baram-Pinto, D.; Shukla, S.; Perkas, N.; Gedanken, A.; Sarid, R. Inhibition of Herpes Simplex Virus Type 1 Infection by Silver Nanoparticles Capped with Mercaptoethane Sulfonate. *Bioconjugate Chem.* **2009**, *20*, 1497−1502.
(23) Chen, M.; Feng, Y.-G.; Wang, X.; Li, T.-C.; Zhang, J.-Y.; Qian, D.-J. Silver Nanoparticles Capped by Oleylamine:Formation, Growth, and Self-Organization. *Langmuir* **2007**, *23*, 5296−5304.
(24) Khan, Z.; Al-Thabaiti, S. A.; Obaid, A. Y.; Khan, Z. A.; Al-Youbi, A. O. Effects of Solvents on the Stability and Morphology of CTAB-Stabilized Silver Nanoparticles. *Colloids Surf., A* **2011**, *390*, 120−125.
(25) Mohanty, S.; Mishra, S.; Jena, P.; Jacob, B.; Sarkar, B.; Sonawane, A. An Investigation on the Antibacterial, Cytotoxic, and Antibiofilm Efficacy of Starch-Stabilized Silver Nanoparticles. *Nanomed. Nanotechnol.* **2012**, *8*, 916−924.
(26) Manna, A.; Imae, T.; Aoi, K.; Okada, M.; Yogo, T. Synthesis of Dendrimer-Passivated Noble Metal Nanoparticles in a Polar Medium: Comparison of Size between Silver and Gold Particles. *Chem. Mater.* **2001**, *13*, 1674−1681.
(27) Zhang, Z.; Patel, R. C.; Kothari, R.; Johnson, C. P.; Friberg, S. E.; Aikens, P. A. Stable Silver Clusters and Nanoparticles Prepared in Polyacrylate and Inverse Micellar Solutions. *J. Phys. Chem. B* **2000**, *104*, 1176−1182.
(28) Zhang, Z.; Han, M. One-Step Preparation of Size-Selected and Well-Dispersed Silver Nanocrystals in Polyacrylonitrile by Simultaneous Reduction and Polymerization. *J. Mater. Chem.* **2003**, *13*, 641−643.
(29) Song, J.; Kang, H.; Lee, C.; Hwang, S. H.; Jang, J. Aqueous Synthesis of Silver Nanoparticle Embedded Cationic Polymer Nanofibers and Their Antibacterial Activity. *ACS Appl. Mater. Interfaces* **2012**, *4*, 460−465.
(30) Gabriel, G. J.; Madkour, A. E.; Dabkowski, J. M.; Nelson, C. F.; Nusslein, K.; Tew, G. N. Synthetic Mimic of Antimicrobial Peptide with Nonmembrane-Disrupting Antibacterial Properties. *Biomacromolecules* **2008**, *9*, 2980−2983.
(31) Ilker, M. F.; Nuesslein, K.; Tew, G. N.; Coughlin, E. B. Tuning the Hemolytic and Antibacterial Activities of Amphiphilic Polynorbornene Derivatives. *J. Am. Chem. Soc.* **2004**, *126*, 15870−15875.
(32) Sakai, N.; Futaki, S.; Matile, S. Anion Hopping of (and on) Functional Oligoarginines: from Chloroform to Cells. *Soft Matter* **2006**, *2*, 636−641.
(33) Nishihara, M.; Perret, F.; Takeuchi, T.; Futaki, S.; Lazar, A. N.; Coleman, A. W.; Sakai, N.; Matile, S. Arginine Magic with New Counterions up the Sleeve. *Org. Biomol. Chem.* **2005**, 31659−1669.
(34) Kolonko, E. M.; Pontrello, J. K.; Mangold, S. L.; Kiessling, L. L. General Synthetic Route to Cell-Permeable Block Copolymers via ROMP. *J. Am. Chem. Soc.* **2009**, *131*, 7327−7333.
(35) Wender, P. A.; Mitchell, D. J.; Pattabiraman, K.; Pelkey, E. T.; Steinman, L.; Rothbard, J. B. The Design, Synthesis, and Evaluation of Molecules That Enable or Enhance Cellular Uptake: Peptoid Molecular Transporters. *Proc. Natl. Acad. Sci. U. S. A.* **2000**, *97*, 13003−13008.
(36) Hennig, A.; Gabriel, G. J.; Tew, G. N.; Matile, S. Stimuli-Responsive Polyguanidino-Oxanorbornene Membrane Transporters as Multicomponent Sensors in Complex Matrices. *J. Am. Chem. Soc.* **2008**, *130*, 10338−10344.
(37) Som, A.; Reuter, A.; Tew, G. N. Protein Transduction Domain Mimics: The Role of Aromatic Functionality. *Angew. Chem., Int. Ed.* **2012**, *51*, 980−983.
(38) Sambhy, V.; MacBride, M. M.; Peterson, B. R.; Sen, A. Silver Bromide Nanoparticle/Polymer Composites: Dual Action Tunable Antimicrobial Materials. *J. Am. Chem. Soc.* **2006**, *128*, 9798−9808.
(39) Aymonier, C.; Schlotterbeck, U.; Antonietti, L.; Zacharias, P.; Thomann, R.; Tiller, J. C.; Mecking, S. Hybrids of Silver Nanoparticles with Amphiphilic Hyperbranched Macromolecules Exhibiting Antimicrobial Properties. *Chem. Commun. (Cambridge, U. K.)* **2002**, 3018−3019.
(40) Liu, J.; Qin, G.; Raveendran, P.; Ikushima, Y. Facile "Green" Synthesis, Characterization, and Catalytic Function of β-D-Glucose-Stabilized Au Nanocrystals. *Chem.—Eur. J.* **2006**, *12*, 2131−2138.
(41) Murugadoss, A.; Chattopadhyay, A. Surface Area Controlled Differential Catalytic Activities of One-Dimensional Chain-like Arrays of Gold Nanoparticles. *J. Phys. Chem. C* **2008**, *112*, 11265−11271.
(42) Goia, D. V. Preparation and Formation Mechanisms of Uniform Metallic Particles in Homogeneous Solutions. *J. Mater. Chem.* **2004**, *14*, 451−458.
(43) Medina-Ramirez, I.; Bashir, S.; Luo, Z.; Liu, J. L. Green Synthesis and Characterization of Polymer-Stabilized Silver Nanoparticles. *Colloids Surf., B* **2009**, *73*, 185−191.
(44) Michna, A.; Adamczyk, Z.; Owieja, M.; Bielaska, E. Kinetics of Silver Nanoparticle Deposition onto Poly(ethylene imine) Modified Mica Determined by AFM and SEM Measurements. *Colloids Surf., A* **2011**, *377*, 261−268.
(45) Yap, F. L.; Thoniyot, P.; Krishnan, S.; Krishnamoorthy, S. Nanoparticle Cluster Arrays for High-Performance SERS through Directed Self-Assembly on Flat Substrates and on Optical Fibers. *ACS Nano* **2012**, *6*, 2056−2070.
(46) Yang, J.; Lee, J. Y.; Too, H.-P. Core-Shell Ag-Au Nanoparticles from Replacement Reaction in Organic Medium. *J. Phys. Chem. B* **2005**, *109*, 19208−19212.
(47) Kim, Y.-K.; Han, S. W.; Min, D.-H. Graphene Oxide Sheath on Ag Nanoparticle/Graphene Hybrid Films as an Antioxidative Coating and Enhancer of Surface-Enhanced Raman Scattering. *ACS Appl. Mater. Interfaces* **2012**, *4*, 6545−6551.
(48) Brown, W. *Dynamic Light Scattering: The Method and Some Applications*; Clarendon Press: Oxford, 1993.
(49) Baalousha, M.; Lead, J. R. Rationalizing Nanomaterial Sizes Measured by Atomic Force Microscopy, Flow Field-Flow Fractionation, and Dynamic Light Scattering: Sample Preparation, Polydispersity, and Particle Structure. *Environ. Sci. Technol.* **2012**, *46*, 6134−6142.
(50) Stamplecoskie, K. G.; Scaiano, J. C.; Tiwari, V. S.; Anis, H. Optimal Size of Silver Nanoparticles for Surface-Enhanced Raman Spectroscopy. *J. Phys. Chem. C* **2011**, *115*, 1403−1409.
(51) Vimala, K.; Mohan, Y. M.; Sivudu, K. S.; Varaprasad, K.; Ravindra, S.; Reddy, N. N.; Padma, Y.; Sreedhar, B.; MohanaRaju, K. Fabrication of Porous Chitosan Films Impregnated with Silver Nanoparticles: A Facile Approach for Superior Antibacterial Application. *Colloids Surf., B* **2010**, *76*, 248−258.
(52) Mahato, M.; Pal, P.; Tah, B.; Ghosh, M.; Talapatra, G. B. Study of Silver Nanoparticle-Hemoglobin Interaction and Composite Formation. *Colloids Surf., B* **2011**, *88*, 141−149.
(53) Gole, A.; Orendorff, C. J.; Murphy, C. J. Immobilization of Gold Nanorods onto Acid-Terminated Self-Assembled Monolayers via Electrostatic Interactions. *Langmuir* **2004**, *20*, 7117−7122.
(54) An, Q.; Yu, M.; Zhang, Y.; Ma, W.; Guo, J.; Wang, C. Fe_3O_4@Carbon Microsphere Supported Ag-Au Bimetallic Nanocrystals with the Enhanced Catalytic Activity and Selectivity for the Reduction of Nitroaromatic Compounds. *J. Phys. Chem. C* **2012**, *116*, 22432−22440.
(55) Chi, Y.; Yuan, Q.; Li, Y.; Tu, J.; Zhao, L.; Li, N.; Li, X. Synthesis of Fe_3O_4@SiO_2-Ag Magnetic Nanocomposite Based on Small-Sized and Highly Dispersed Silver Nanoparticles for Catalytic Reduction of 4-Nitrophenol. *J. Colloid Interface Sci.* **2012**, *383*, 96−102.
(56) Rashid, M. H.; Mandal, T. K. Synthesis and Catalytic Application of Nanostructured Silver Dendrites. *J. Phys. Chem. C* **2007**, *111*, 16750−16760.
(57) Shin, K. S.; Cho, Y. K.; Choi, J.-Y.; Kim, K. Facile Synthesis of Silver-Deposited Silanized Magnetite Nanoparticles and Their

Application for Catalytic Reduction of Nitrophenols. *Appl. Catal., A* **2012**, *413*−*414*, 170−175.
(58) Zhang, J.; Chen, G.; Chaker, M.; Rosei, F.; Ma, D. Gold Nanoparticle Decorated Ceria Nanotubes with Significantly High Catalytic Activity for the Reduction of Nitrophenol and Mechanism Study. *Appl. Catal., B* **2013**, *132*−*133*, 107−115.
(59) Wunder, S.; Polzer, F.; Lu, Y.; Mei, Y.; Ballauff, M. Kinetic Analysis of Catalytic Reduction of 4-Nitrophenol by Metallic Nanoparticles Immobilized in Spherical Polyelectrolyte Brushes. *J. Phys. Chem. C* **2010**, *114*, 8814−8820.
(60) Liu, B. H.; Li, Z. P. A Review: Hydrogen Generation from Borohydride Hydrolysis Reaction. *J. Power Sources* **2009**, *187*, 527−534.
(61) Vannice, M. A. *Reactions*; Springer Science + Business Media: Philadelphia, PA, 2005.
(62) Guella, G.; Patton, B.; Miotello, A. Kinetic Features of the Platinum Catalyzed Hydrolysis of Sodium Borohydride from ^{11}B NMR Measurements. *J. Phys. Chem. C* **2007**, *111*, 18744−18750.
(63) Lin, J.-J.; Lin, W.-C.; Li, S.-D.; Lin, C.-Y.; Hsu, S.-h. Evaluation of the Antibacterial Activity and Biocompatibility for Silver Nanoparticles Immobilized on Nano Silicate Platelets. *ACS Appl. Mater. Interfaces* **2013**, *5*, 433−443.
(64) Santos, K. d. O.; Elias, W. C.; Signori, A. M.; Giacomelli, F. C.; Yang, H.; Domingos, J. B. Synthesis and Catalytic Properties of Silver Nanoparticle Linear Polyethylene Imine Colloidal Systems. *J. Phys. Chem. C* **2012**, *116*, 4594−4604.
(65) Lin, S.; Cheng, Y.; Liu, J.; Wiesner, M. R. Polymeric Coatings on Silver Nanoparticles Hinder Autoaggregation but Enhance Attachment to Uncoated Surfaces. *Langmuir* **2012**, *28*, 4178−4186.